

# Excitatory and suppressive receptive field subunits in awake monkey primary visual cortex (V1)

Xiaodong Chen\*, Feng Han†, Mu-ming Poo\*<sup>§</sup>, and Yang Dan<sup>†\*§</sup>

\*Institute of Neuroscience, State Key Laboratory of Neuroscience, Shanghai Institutes for Biological Sciences, Chinese Academy of Sciences, 320 Yue-Yang Road, Shanghai 200031, China; †Group in Vision Science, University of California, Berkeley, CA 94720; and <sup>§</sup>Helen Wills Neuroscience Institute and Department of Molecular and Cell Biology, University of California, Berkeley, CA 94720

Edited by Charles F. Stevens, The Salk Institute for Biological Studies, La Jolla, CA, and approved October 15, 2007 (received for review July 25, 2007)

**An essential step in understanding visual processing is to characterize the neuronal receptive fields (RFs) at each stage of the visual pathway. However, RF characterization beyond simple cells in the primary visual cortex (V1) remains a major challenge. Recent application of spike-triggered covariance (STC) analysis has greatly facilitated characterization of complex cell RFs in anesthetized animals. Here we apply STC to RF characterization in awake monkey V1. We found up to nine subunits for each cell, including one or two dominant excitatory subunits as described by the standard model, along with additional excitatory and suppressive subunits with weaker contributions. Compared with the dominant subunits, the nondominant excitatory subunits prefer similar orientations and spatial frequencies but have larger spatial envelopes. They contribute to response invariance to small changes in stimulus orientation, position, and spatial frequency. In contrast, the suppressive subunits are tuned to orientations 45°–90° different from the excitatory subunits, which may underlie cross-orientation suppression. Together, the excitatory and suppressive subunits form a compact description of RFs in awake monkey V1, allowing prediction of the responses to arbitrary visual stimuli.**

The response properties of primary visual cortical (V1) neurons have been studied extensively over the past several decades. In the standard model, a simple cell receptive field (RF) consists of alternating ON and OFF subregions, which directly correspond to the orientation and spatial-frequency tuning of the cell (1, 2). Complex cells exhibit orientation and spatial-frequency tuning similar to simple cells, but they are insensitive to the contrast polarity and stimulus position within the RF. The energy model for complex cell RF consists of a pair of simple-cell-like subunits with the same orientation and spatial-frequency tuning but different ON/OFF phases (3, 4). This model accounts for the phase invariance as well as stimulus selectivity of complex cells.

To validate such RF models and to predict the neuronal responses to arbitrary visual stimuli, it is necessary to measure the RF structure quantitatively. For simple cells, spike-triggered average (STA) has been used effectively to estimate their RFs from the responses to sparse noise (5) or white noise (6). For complex cells, however, because the outputs of different RF subunits are combined nonlinearly, these subunits cannot be estimated by STA. In previous studies, complex cell RFs have been studied by measuring the nonlinear interaction between paired stimuli (3, 7, 8). Another method used in recent studies is spike-triggered covariance (STC) analysis (9, 10). Instead of averaging all of the stimuli preceding spikes (as in STA), in STC analysis one computes the covariance matrix of the spike-triggered stimulus ensemble and identifies the eigenvectors with eigenvalues significantly different from those of the entire stimulus ensemble. This method can reveal stimulus features that drive the neuron in a contrast-dependent but polarity-invariant manner, and it has proved highly effective in characterizing complex cell RF subunits in both cat (11, 12) and monkey (13) V1.

Although the above studies have characterized the spatiotemporal structure of complex cell RFs in anesthetized animals, an ultimate challenge is to understand RF properties in the awake

brain. Neuronal RFs in awake monkey V1 have been studied in phase-separated Fourier space (14). In the current study, we used STC to analyze the spatial structure of V1 RFs in awake monkeys. In addition to the dominant subunits that are consistent with the standard models for simple (1, 2) and complex (3, 4) cells, we found additional excitatory subunits that contribute to orientation, position, and spatial-frequency invariance. For some cells, we also found suppressive subunits (13). These subunits are tuned to orientations up to 90° different from the excitatory subunits, which may contribute to cross-orientation suppression (15). Including the nondominant excitatory and suppressive subunits in the model significantly improved the prediction of neuronal responses to arbitrary white noise stimuli.

## Results

We made single-unit recordings from 227 V1 neurons in three macaque monkeys performing a fixation task. Visual stimuli were binary white noise ( $10 \times 10 - 12 \times 12$  pixels, 25 frames per s) presented in an area slightly larger than the RF of each cell. During each stimulus epoch (7,500 frames, 5 min), the eye position was monitored continuously. Recordings during periods when the eye position was outside of a fixation window were excluded from analyses (Fig. 1A).

The stimulus preceding each spike was collected to form the spike-triggered ensemble (Fig. 1B), and the covariance matrix of this ensemble was computed. Significant eigenvalues were defined as those that were significantly different from (i) the control eigenvalues calculated based on randomized spike trains (Fig. 2A) and (ii) their neighboring eigenvalues (Fig. 2B; *Materials and Methods*) (16). For 145 of the 227 cells studied, we found at least one significant eigenvalue. The eigenvectors with significantly higher eigenvalues represent stimulus features that excite the cell (11, 16), whereas those with significantly lower eigenvalues reflect suppressive features that reduce neuronal firing (13).

**Grouping of Significant Eigenvectors.** The significant eigenvectors of each cell could be divided into three groups, based on their spatial structure and eigenvalues. The first group consisted of one or two eigenvectors whose eigenvalues stood out most prominently above the rest. These excitatory eigenvectors, referred to as “dominant eigenvectors,” were almost always Gabor-like. Most of the complex cell-like neurons, whose responses to drifting gratings were modulated only weakly at the stimulus temporal frequency (17), contained a pair of dominant eigenvectors (e.g., both cells in Fig. 2). These eigenvectors were similar to each other in size, orientation, and spatial frequency, but different in phase (Fig. 2C), consistent with the pair of subunits in the energy model (3, 4). On the other

Author contributions: X.C., M.-m.P., and Y.D. designed research; X.C. performed research; X.C., F.H., and Y.D. analyzed data; and X.C., M.-m.P., and Y.D. wrote the paper.

The authors declare no conflict of interest.

This article is a PNAS Direct Submission.

<sup>§</sup>To whom correspondence may be addressed. E-mail: mpoo@berkeley.edu or ydan@berkeley.edu.

© 2007 by The National Academy of Sciences of the USA

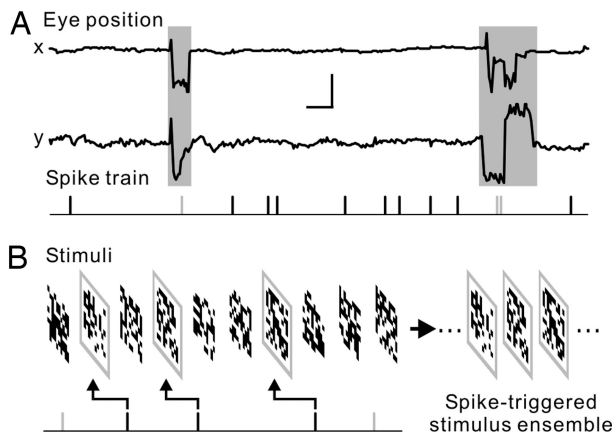


**Fig. 1.** Illustration of experimental and analytical procedures. (A) Example eye position traces recorded by the eye tracker. (Scales: 1 s, 1°.) Shading: periods with eye position outside of fixation window. Corresponding segments of the spike train (bottom) were excluded from analysis. Gray: excluded spikes. (B) White noise stimuli. Gray box: stimulus preceding each spike.

hand, cells with strong temporal modulations (simple-cell-like) are likely to have a single dominant eigenvector (i.e., the largest jump is between the first and second eigenvalues). This eigenvector typically resembled STA (data not shown), which represents the linear RF of the simple cell. Note that we did not strictly distinguish between simple and complex cells because recent studies suggested that V1 neurons fall on a simple/complex continuum rather than in two distinct classes (18, 19).

Many simple- or complex-like neurons also exhibited additional excitatory eigenvectors, whose eigenvalues showed smaller but significant upward jumps (Fig. 2*A* and *B*). This second group of eigenvectors, referred to as “nondominant” excitatory eigenvectors, were oriented similarly to the dominant eigenvectors but showed more complex spatial structures and larger sizes (Figs. 2*C* and 3*A*). For 38 cells, we also found a third group of eigenvectors with significantly lower eigenvalues. Most of these suppressive eigenvectors (Fig. 2*C*, second cell; Fig. 3*A*, third and fourth cells) are oriented differently from the excitatory eigenvectors. It is important to note that, although the significant eigenvectors provide a functional description of the RF that is indicative of the response properties of the presynaptic neurons, each significant eigenvector does not necessarily represent the RF of an individual presynaptic cell (i.e., an “anatomical subunit”). Instead, it is likely to represent a linear combination of multiple anatomical subunits (11, 13). However, as a convenient functional description, we refer to these significant eigenvectors as the excitatory or suppressive RF subunits.

**Relationship Between Subunit Groups.** To understand the relationship between the three groups of subunits, we first compared their locations and sizes by computing the pooled spatial envelope of each group (square root of the weighted sum of squares of all of the subunits in each group; see *Materials and Methods*) (13). Compared with the dominant group, the nondominant excitatory subunits showed a larger spatial envelope (Fig. 4*A* and *C*), similar to the finding in anesthetized monkey V1 (13). This finding could be explained if the nondominant eigenvectors represent combinations of multiple anatomical subunits that are spatially displaced from each other. The suppressive subunits, on the other hand, largely overlapped with the dominant subunits in space. Quantitative comparison of the subunit sizes is summarized in Fig. 5*A* and *B*, based on the width at half height of each pooled envelope along the preferred orientation (length) and the perpendicular axis (width).

We also compared the spatial-frequency and orientation tuning

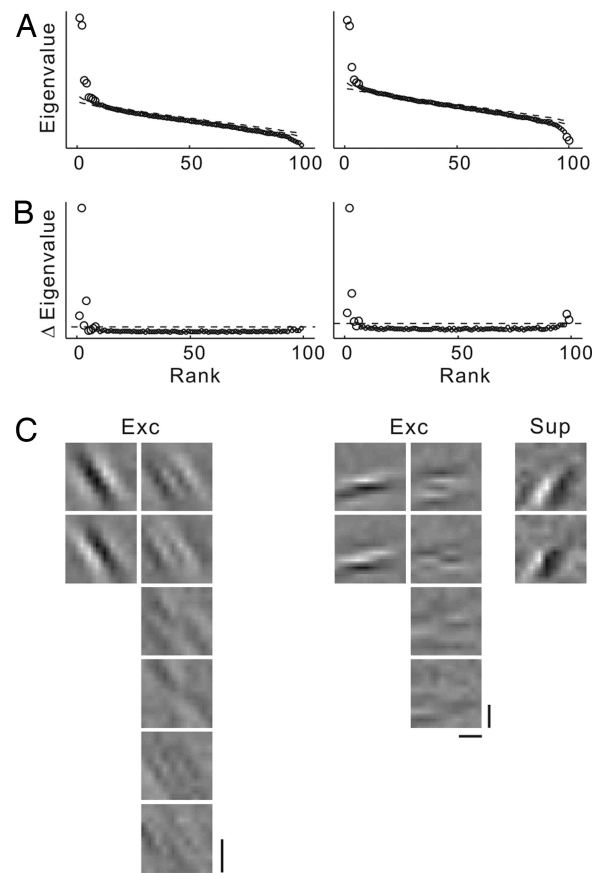


**Fig. 2.** Identification of significant eigenvectors, illustrated with two V1 cells (*Left* and *Right*). (A) Eigenvalues of STC matrix. Dashed lines: control confidence intervals ( $P < 10^{-4}$ ). (B) Difference between neighboring eigenvalues. Dashed line: confidence interval for the difference ( $P < 10^{-4}$ ). (A and B) Large circles represent significant eigenvalues satisfying criteria. (C) Significant eigenvectors. Contrast of each eigenvector is scaled by its relative weight (see *Materials and Methods*). Excitatory and suppressive eigenvectors were scaled separately. (Scale: 0.5°.)

of the three groups based on the pooled spatial spectrum of each group (Fig. 4*B*). The spectrum of the nondominant excitatory group largely overlapped with that of the dominant group (Fig. 4*C*), indicating similar orientation and frequency tuning. In contrast, the spectrum of the suppressive subunits showed little overlap with the excitatory groups. The separation between the excitatory and suppressive subunits in spatial spectrum was more pronounced along the angular axis than the radial axis, indicating major differences in orientation as opposed to frequency tuning. For the population of cells, the preferred spatial frequency and orientation of the nondominant excitatory subunits were closely correlated with those of the dominant subunits (Fig. 5*C Upper* and *D Upper*), but the suppressive subunits showed larger deviations in frequency tuning and up to 90° difference in preferred orientation (Fig. 5*C Lower* and *D Lower*).

**Response Invariance.** The angular separation between the excitatory and suppressive subunits in the spectral domain suggests that the suppressive subunits contribute to cross-orientation suppression (15), which should enhance the selectivity of V1 neurons. What is the function of the nondominant excitatory subunits? Because each excitatory eigenvector is likely to represent a combination of multiple anatomical subunits (11, 13), and conversely an anatomical subunit may be approximated as a combination of eigenvectors, we examined various linear combinations of the excitatory eigenvectors

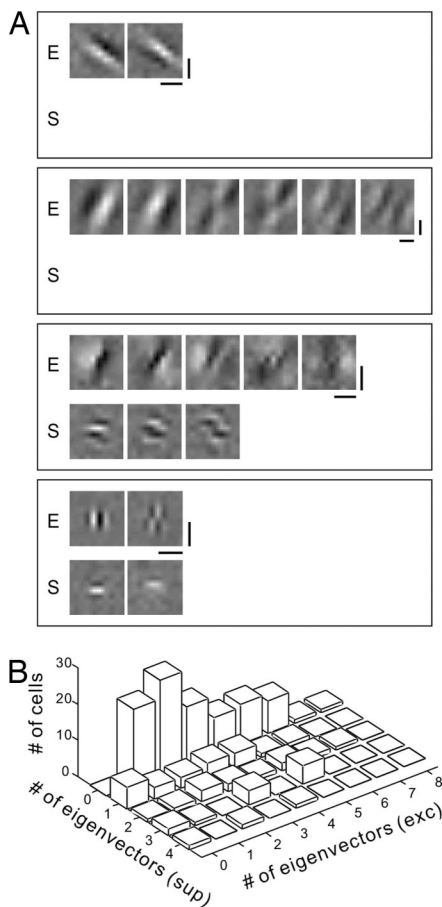


**Fig. 3.** Number of significant eigenvectors per cell. (A) Significant eigenvectors for four example cells. E, excitatory; S, suppressive. (Scale:  $0.5^\circ$ .) (B) Distribution of the number of significant eigenvectors per cell.

tors. The neuronal responses to combinations of eigenvectors can be characterized by joint contrast–response functions (11, 13).

Fig. 6A shows the joint contrast–response functions for four pair-wise combinations of the excitatory subunits of a neuron. The contrast of a given subunit in each stimulus is defined as the dot product of the eigenvector and the stimulus, and the neuronal firing rate is plotted against the contrasts of each pair of subunits. Consistent with previous findings in cat V1 (11), each combination of the dominant pair of subunits also is Gabor-like (Fig. 6A Upper Left), with the spatial phase shifting with the relative weights of the two subunits (angular coordinate of the 2-D function). The circularly symmetric joint contrast–response function thus is consistent with the known phase invariance of complex cells (1, 3, 4). Interestingly, combinations between a dominant and a nondominant excitatory subunit revealed other forms of invariance. For this cell, although the third (nondominant) eigenvector contained fractured ON and OFF subregions, its combinations with the first (dominant) eigenvector resulted in Gabor-like patterns at different orientations (Fig. 6A Upper Right, compare patterns in the three boxes). Furthermore, combinations between the second and third eigenvectors resulted in Gabor patterns at different positions (Fig. 6A Lower Left), and those between the second and fifth exhibited different frequencies (Fig. 6A Lower Right). Because the nondominant subunits make weaker contributions to the response than the dominant ones do, the joint contrast–response functions did not exhibit perfect circular symmetry. Nevertheless, the existence of these weaker excitatory subunits enhanced the response invariance with respect to small changes in stimulus orientation, position, and

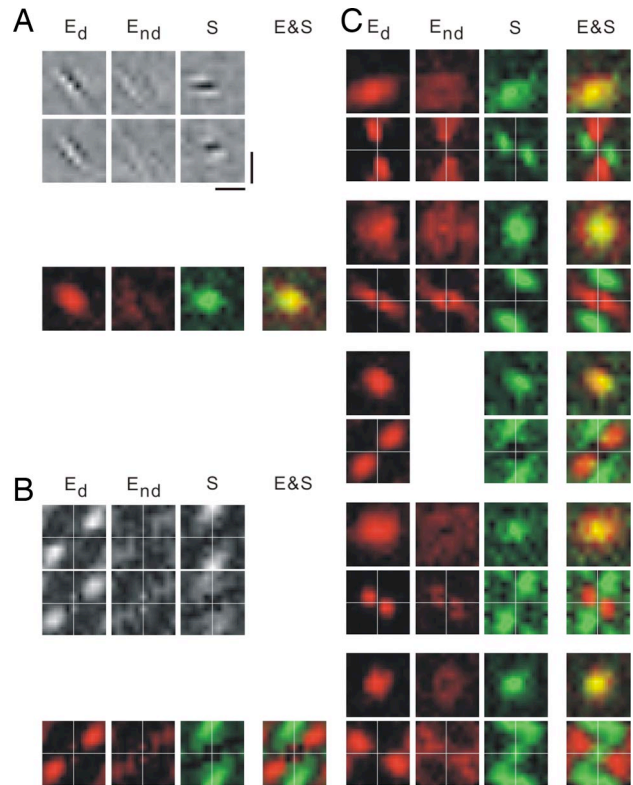


**Fig. 4.** Spatial and spectral relationships among subunit groups. (A) (Upper) Dominant and nondominant excitatory ( $E_d$  and  $E_{nd}$ ) and suppressive (S) subunits of a cell. (Scale:  $0.5^\circ$ .) (Lower) Pooled spatial envelope of each group of subunits. Red, E; green, S. In E&S (all groups superimposed), yellow indicates overlap between E and S. (B) (Upper) Spatial-frequency spectrum of each subunit in A. (Lower) Pooled frequency spectrum of each group. (C) Pooled spatial envelopes (upper rows) and frequency spectra (lower rows) of the three subunit groups for five cells.

frequency (20). A plausible anatomical basis for such invariance is that the neuron receives inputs from a set of presynaptic neurons with slightly different preferred orientations, RF positions, and spatial frequencies.

The above three types of invariance also were observed in other cells, with orientation invariance the most common. We thus further quantified the effect of nondominant excitatory subunits on orientation tuning. The tuning of each subunit was computed as its responses to sinusoidal gratings at a range of orientations at the optimal frequency. Because previous studies have shown that the excitatory subunits contribute additively to the responses (11, 13), the tuning of the cell was predicted as the weighted sum of the tuning of all excitatory subunits, with the weight of each subunit proportional to its contrast–response gain (*Materials and Methods*). As shown in Fig. 6B, including the nondominant excitatory subunits in the prediction indeed broadened the tuning for this example cell. For the population of cells with well tuned excitatory subunits, including the nondominant subunits significantly increased the width of tuning (Fig. 6C,  $P < 0.01$ , Wilcoxon signed rank test). Notably, the effects of the nondominant excitatory subunits and the suppressive subunits on orientation tuning do not simply cancel each other. Although the nondominant excitatory subunits render the neuron less sensitive to small variations around the optimal orientation, the suppressive subunits reduce the responses near the orthogonal orientation without necessarily narrowing the tuning curve (Fig. 6B Inset).

**Predictions of Responses to White Noise.** Finally, to assess the RF model based on the significant eigenvectors, we predicted the

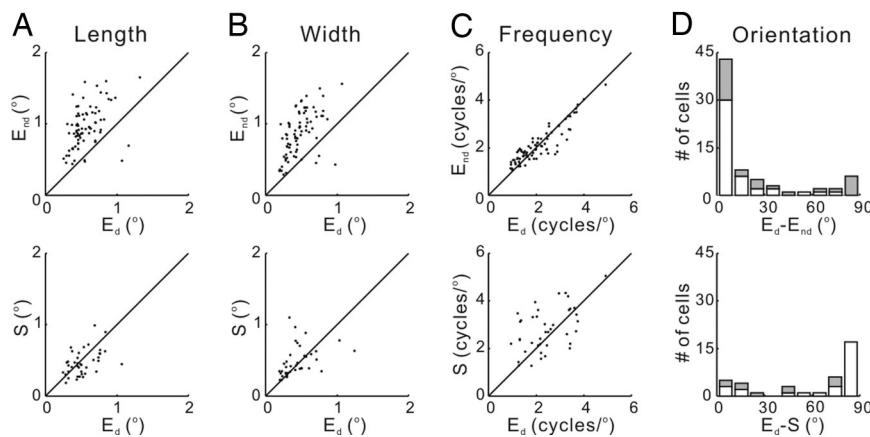


**Fig. 5.** Quantitative comparison between nondominant and dominant subunits. (A and B) Length and width of pooled spatial envelope, measured by width at half height. Each point represents one cell ( $n = 79$ ). (C) Optimal spatial frequency (peak of frequency spectrum) for the same cells in A and B. (D) Difference in preferred orientation. White bars, cells with clear tuning (circular variance of tuning for each group of subunits  $< 0.7$ ); gray bars, poorly tuned cells (circular variance  $> 0.7$ ). Circular variance is defined as  $1 - |\sum_k R_k e^{i2\theta_k}| / \sum_k R_k$  ( $R_k$ , response at orientation  $\theta_k$ ,  $0 < \theta_k < 180^\circ$ ).

response of each cell to a short white noise test sequence (30 s, repeated 4–70 times) by using (i) dominant subunits alone, (ii) all excitatory subunits, and (iii) all excitatory and suppressive subunits. The responses of the excitatory subunits and those of the suppressive subunits first were summed separately by using weights proportional to their contrast–response gains. The excitatory and suppressive components then were combined with a nonlinear function that allows both subtractive and divisive interactions (13) (*Materials and Methods*). Fig. 7A shows the measured response of an example cell (gray shading) and the predictions based on the dominant subunits alone (black line) and based on all excitatory and suppressive subunits (red line). Although the model based on the dominant subunits alone predicted the main temporal variations of the response, including the nondominant excitatory and suppressive subunits improved the prediction by alleviating both underestimation and overestimation of the peak amplitudes (Fig. 7A, arrowheads).

We measured the quality of prediction by each model using the correlation coefficient between the predicted and measured responses. Compared with the model based on the dominant subunits alone, including the nondominant excitatory subunits significantly improved the prediction for the population of cells (Fig. 7B,  $P < 10^{-5}$ , Wilcoxon signed rank test,  $n = 83$ ). Including the suppressive subunits led to a small further improvement (Fig. 7C), although the effect was not significant. Even with the full model, however, the correlation coefficient between the predicted and measured responses was lower than that between measured responses averaged from different repeats (Fig. 7D), indicating that the prediction error could not be entirely accounted for by noise in the measured responses. The incompleteness of the model may be attributable to additional subunits not identified by STC or to inaccuracy in the estimated RF subunits, both of which depend on the amount of data (21, 22), which is limited in recordings from awake monkeys. More importantly, the responses are likely to exhibit other forms of nonlinearity such as adaptation (23), which are not captured by the RF model used in this study.

## Discussion

The current study, together with several other STC analyses (11–13, 16), suggests the following model for V1 classical RF. The dominant RF component is a Gabor-like subunit for simple cells and a pair of subunits for complex cells, consistent with the standard model (1–4). In both anesthetized and awake monkeys, however, STC analysis allowed identification of two additional groups of subunits: the nondominant excitatory and suppressive subunits, whose con-

tributions to V1 responses are weaker than those of the dominant subunits. The nondominant excitatory subunits are more dispersed spatially but largely overlap with the dominant subunits in the frequency spectrum (Figs. 4 and 5), and they contribute to response invariance to small changes in stimulus orientation, position, and frequency (Fig. 6). In contrast, the suppressive subunits overlap with the dominant subunits spatially but are complementary in the frequency spectrum. They are likely to mediate suppression of the responses to “antagonistic” visual features such as those at the orthogonal orientation (Figs. 4 and 5). Invariance and selectivity of neuronal responses are both important for visual processing. As shown in Fig. 7, incorporating the nondominant subunits in the model improves the prediction of responses to arbitrary white noise stimuli.

In previous studies in anesthetized cat V1 (11, 12, 16), we found that most complex cell RFs consist of two Gabor-like subunits, and nondominant subunits rarely were observed. In this study, it is possible that small eye movements within the fixation window produced artifactual, significant eigenvectors and contributed to the nondominant subunits. Although we cannot exclude this possibility completely, the finding that the nondominant subunits significantly improved the response prediction (Fig. 7) indicates that they are integral components of the functional description of V1 responses. The difference in the number of significant eigenvectors found in the current and previous studies may be partly attributable to differences in the number of spikes used in the analysis, the signal-to-noise ratio of the responses, or the number or strength of the nondominant subunits. Regardless of the underlying reason, the fact that nondominant subunits are readily observed in V1 of both anesthetized (13) and awake monkeys suggests that there are significant interspecies differences in the number of RF subunits identifiable by the STC analysis.

The effect of the nondominant subunits in improving response prediction found in this study (Fig. 7) is relatively small compared with that found in anesthetized monkey V1 (13). This discrepancy may be partly attributable to the difference in the stimuli used for testing the models. Although we used arbitrary white noise stimuli, the test stimuli previously used were matched to the nondominant subunits in spatiotemporal patterns and thus were likely to emphasize their contributions to the responses. It also is possible that, compared with the 2-D white noise stimuli used in this study, the relative contribution of the nondominant subunits is stronger in response to bar stimuli at the preferred orientation (13). Nevertheless, it is interesting to note that both null-direction and cross-orientation suppression can be modeled by suppressive RF sub-

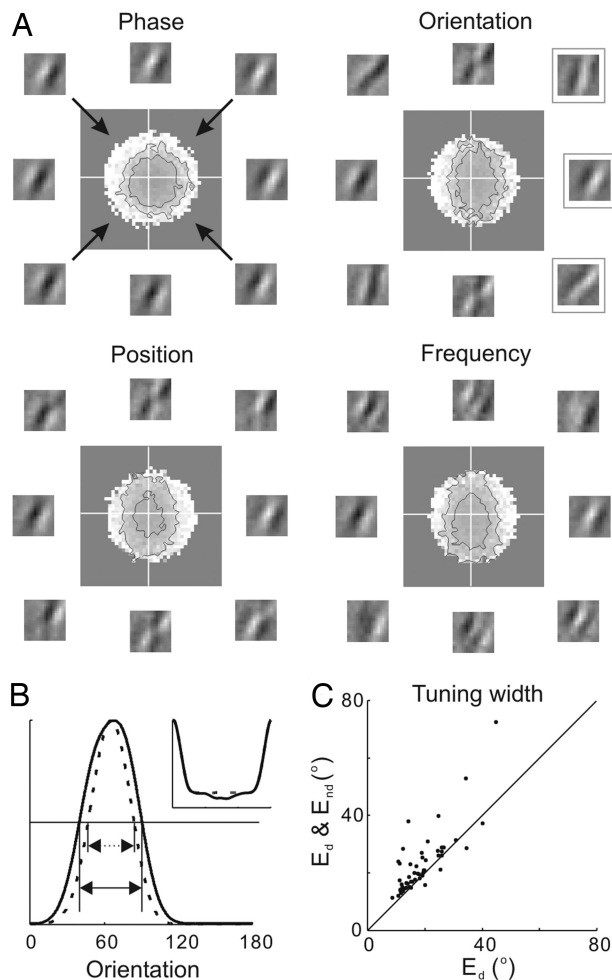


**Fig. 6.** Phase, orientation, position, and frequency invariance. (A) Joint contrast–response functions of a complex cell (second cell in Fig. 3A) for different pair-wise combinations of its six excitatory subunits. Firing rate is luminance-coded. Black lines indicate contours of constant firing rate (at  $0.5\times$  and  $1\times$  mean of each function); circular contour indicates perfect invariance. Small outer plots represent stimulus patterns corresponding to selected points (arrows) in the function. (B) Orientation tuning of the cell predicted by the dominant subunits alone (dashed line) and by all excitatory subunits (solid line). Arrows indicate width at half height. (Inset) Predicted tuning of another cell, based on only the excitatory subunits (dashed line) and on both excitatory and suppressive subunits. (C) Predicted tuning width based on all excitatory subunits versus that based on dominant subunits alone. Each point represents one cell; only cells with clear tuning (circular variance  $< 0.6$ ) were included ( $n = 56$ ).

units, even though they are likely to be mediated by distinct neural circuits.

Most of the previous quantitative studies of neuronal RFs were performed under anesthesia, which may significantly affect the response properties of sensory neurons. Our study shows that STC analysis is highly effective for mapping RF subunit structure in awake monkey V1. Although this study is performed with white noise stimuli, a similar technique can be used to analyze cortical responses to naturalistic stimuli (12, 14, 16, 24). The findings reported here not only provide a compact RF model for understanding V1 responses to arbitrary stimuli (Fig. 7) but also set the stage for studying nonlinear visual processing in higher-level cortical areas.

## Materials and Methods

**Recording.** Single-unit recordings were made in V1 of three adult monkeys (two male and one female *Macaca mulatta*) by using

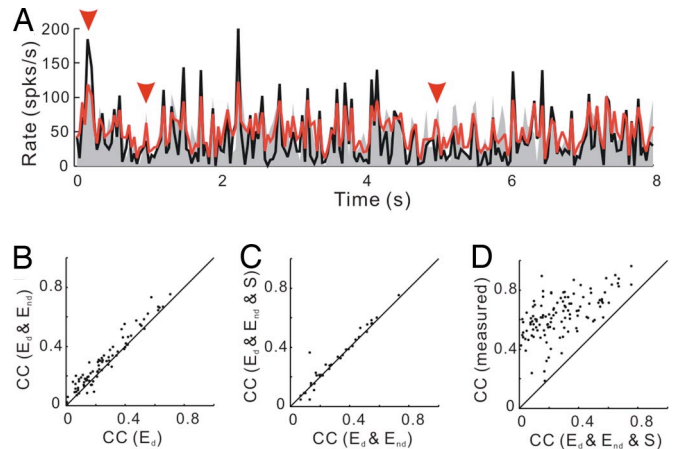


**Fig. 7.** Prediction of responses to white noise stimuli. (A) Comparison of predicted and measured firing rates of a cell. Gray shading: measured response averaged from 24 repeats of the test stimulus. Black line: prediction based on dominant subunits. Red line: Prediction based on all subunits (six excitatory, one suppressive). Red arrowheads, peaks better predicted by the model with all subunits. (B) Improvement of prediction by nondominant excitatory subunits. Correlation coefficient (CC) between measured and predicted responses based on all excitatory subunits versus CC with only dominant subunits. Each symbol represents one cell. (C) Improvement of prediction by suppressive subunits. CC based on both excitatory and suppressive subunits versus CC with only excitatory subunits. (D) CC between measured responses (averaged from two nonoverlapping sets of repeats) versus CC between predicted (based on all subunits) and measured responses ( $n = 123$ ).

glass-coated tungsten electrodes (25). Unit isolation was based on cluster analysis of waveforms and the presence of a refractory period in autocorrelograms. Each recording epoch was 5 min. All single units lasting for  $\geq 3$  epochs were included (maximum 25 epochs,  $n = 227$ ). The RFs of these cells were  $2^\circ$ – $9^\circ$  from the fixation point. During each epoch, the monkey performed a continuous fixation task for a juice reward. Eye position was monitored with a remote infrared eye tracker (EYELINK II, resolution  $0.01^\circ$ , sampling rate 500 Hz). An elliptical window was set for eye position; vertical and horizontal axes were selected so that the kurtosis of data points in the window was 3 (mean vertical axis,  $1.2^\circ$ ; horizontal axis,  $0.5^\circ$ ). Data recorded while the eye position was outside of the window were discarded (Fig. 1). In practice, however, our results were quite insensitive to the window size or shape; results were similar even when it was set to infinity. Surgery was conducted under aseptic conditions under deep pentobarbital anesthesia. All procedures were in accordance with National Institutes of Health guidelines.

**Visual Stimulation.** Stimuli were generated with a PC, presented with a Sony Multiscan G520 monitor ( $30 \times 40$  cm, refresh rate 100 Hz, maximum luminance  $80 \text{ cd/m}^2$ ). Binary white noise ( $10 \times 10 - 12 \times 12$  pixels,  $0.8 \times 0.8^\circ - 4.2 \times 4.2^\circ$ , 100% contrast) was presented at an effective frame rate of 25 Hz (updated every four frames). Each epoch consisted of 7,500 frames, and stimuli in different epochs were different. To test prediction of the model based on significant eigenvectors, a white noise sequence (750 frames, 30 s) was repeated 4–70 times for each cell.

**STC Analysis.** Details of the STC analysis have been described previously (11, 13, 16). Briefly, the STC matrix  $[C_{m,n}]$  was computed as

$$C_{m,n} = \frac{1}{N} \sum_{i=1}^N S_m(i) S_n(i),$$

